P4.9 RADIOMETRIC SIGNATURES OF RAINFALL STRUCTURES FROM THE TROPICAL RAINFALL MEASURING MISSION (TRMM) SENSORS OVER DIFFERENT CLIMATE REGIMES

Dong-Bin Shin * and Long S. Chiu
George Mason University, Fairfax, VA 22030
Alfred T. C. Chang
Goddard Space Flight Center/NASA, Greenbelt, MD 20771

1. INTRODUCTION

Global precipitation is a key component in the global energy and water cycles. Microwave radiometry from space has been used extensively to provide global rainfall information since there is a connection between the measured radiance and the vertical distributions of precipitating hydrometeors. These relations have been exploited by a number of investigators (e.g., Wilheit et al. 1977; Smith and Mugnai 1988; Spencer et al. 1989; Petty 1994; Kummerow et al. 1996; Shin and Kummerow 2002).

There are uncertainties associated with these satellite microwave rainfall estimates. One of the major uncertainties is the so-called beam-filling bias, which arises because of the effect of the inhomogeneity of the rain field within the sensor field of view (FOV) and the non-linear response of the rain rate (R) to brightness temperature (Tb). Chiu et al. (1990) provided an approximate formula for the beam-filling bias, which is associated with the spatial variance of the rain field coupled to the nonlinearity of the algorithm physics and/or sensor response. Uncertainty in the Tb-R relation can be attributed to variability of vertical profiles of precipitating hydrometeors having similar observed microwave radiances.

The data acquired by the Tropical Rainfall Measuring Mission (TRMM) provide an unique opportunity to reassess the beam-filling uncertainty associated with space-borne passive microwave rainfall estimation. TRMM provides almost concomitant observations of microwave radiometric and space-borne radar. In this study, collocated observations of the microwave radiometric Tb from the TRMM Microwave Imager (TMI) and rainfall profile retrieved from the precipitation radar (PR) are examined for different climate regimes. An advantage of this observational approach is that radiometric responses to the uncertainties due to the rain field itself can be retrieved without intervention of additional uncertainties from the other sources such as those that may be introduced by radiative transfer calculations. In addition, the successful operation of the TRMM satellite, now in its fifth year, allows us to construct reliable information about the regional and temporal variation of the radiometric signatures to rainfall structures. The information, thus, can serve as the basis of a more comprehensive error model for passive microwave rainfall retrievals.

2. DATA

The TMI measures the vertical and horizontal microwave radiances (brightness temperatures) emitted by the Earth and Atmosphere at five frequencies (10.7, 19.4, 21.3 (vertical only) 37.0 and 85.5 GHz). The PR operates at 13.8 GHz and measures the return power with a vertical spacing of 250 m for normal samples at a nadir resolution of ~4km and a swath with of 215 km. The details of TRMM standard products can be found in Kummerow et al. (1998).

The data we used are the TMI Tb (or 1B11 as

* *Corresponding author address:* Dong-Bin Shin, George Mason University, Center for Earth Observing and Space Research, School of Computational Sciences, Fairfax, VA 22030; e-mail: dshin@scs.gmu.edu.

referenced by the TRMM Science and Data Information system, TSDIS) and PR rainfall profile (TSDIS referenced 2A25). Our analyses are carried out over sections of the East Pacific (5^o N ~ 15^o N, 150^o W ~ 120^o W) and the West Pacific (130^o E ~ 160E, 2^o N ~ 12^o N) during the period of December 1999 to February 2000. The TMI Tb data are first mapped onto the PR pixels by weighing the appropriate coverage by the TMI channels. The cross-track scanning of the PR and the conical scanning of TMI introduce a maximum time lag of about a minute and a half between the PR and TMI pixels. Different spatial resolutions are dealt with by simply convolving the high-resolution (4 km) Tb and rainfall data. In this study, we use three different FOVs (44 km, 28 km and 12 km), which represent approximately the 10 GHz, 19 GHz and 37 GHz resolutions of the TMI, respectively.

3. RAINFALL INHOMOGENEITY

3.1 *Coefficient of Variation*

The coefficient of variation (CV) or inhomogeneity factor is used to describe spatial (horizontal) inhomogeneity of the rain field observed from the PR. The CV within the FOV is defined as the ratio of standard deviation of rain rate within the FOV to FOV-averaged rain rate (σ / μ). The FOV-averaged rain rate is obtained from the high-resolution PR pixels (4 km) within the FOV. Figure 1 shows the variation of the CV as a function of the FOV-averaged rain rate for the East and West Pacific boxes. The dotted lines in the figures indicate the average CV over all data points. It can be seen that CV increases with the size of the FOV, suggesting a larger beam-filling bias is associated with lower resolution. There is a tendency for the CV at the low rain rates (<10 mm/h for the 12 km and 28 km boxes) to be lower than the average CV, suggesting that the rain fields with weaker rain rates are more homogeneous than boxes with heavier rain. The most homogeneous (lowest CV) rain fields are generally found at the rain rates between 4~7 mm/h for the three different resolutions. The other prominent feature is that the CV at the West Pacific box is consistently higher than the East Pacific boxes at the same FOV. The larger inhomogeneity factor for the West Pacific precipitation system turns out to significantly weaken the physical connection from increasing the liquid content and microwave radiance (more nonlinearity). This will be shown in section 4.

3.2 *Vertical Structures in the Inhomogeneous Spaces*

We next examine variability of the vertical rain profile associated with the same surface rain rate. Figure 2 shows the vertical profiles of rain rate at various CVs that have the same surface rain rate of 2.5 mm/h. It can be seen that the mean profiles are well separated by the inhomogeneity factor: profiles associated with lower CVs tend to show the existence of the bright band, which is indicative of stratiform rain, whereas profiles of high CVs tend to show no bright band, indicative of convective precipitation. We also note that the bright band height (peak of the rain profile) is higher for the West Pacific than that of the East Pacific. The mean rainfall profiles with different surface rain rates (not shown) reveal a similar pattern. In order to demonstrate the connection between the vertical structures and spatial inhomogeneity, we compute a ratio of the total columnar rain rates (ΣR_i) to that at 2 km (R_{2km}). This ratio can be interpreted as the inverse of the rain efficiency. As the ratio decreases, the profiles tend to resemble more convective-like vertical structures. Figure 3 shows 2-dimensional histograms of the ratio and the inhomogeneity factor (CV) for the three FOVs. We noted that the lower ratio (more convective rainfall) tends to be associated with higher CVs. This reinforces that fact that the beam-filling bias is due to the coupling between the spatial inhomogeneity within FOVs and associated vertical structures. These results can be interpreted in light of the first-order formula for the beam-filling bias presented in Chiu et

al. (1990). The formula for the beam-filling bias (δR) is written as

$$\delta R = -\frac{1}{2}\left\{ (R - [R])^2 \frac{Tb''([R])}{Tb'([R])} \right\} \qquad (1)$$

where square brackets denote FOV average. The first term is a property of the rain field only, which is related to the inhomogeneity factor. The second is dependent on the curvature of the R-Tb relation that is mainly determined by the details of vertical structures.

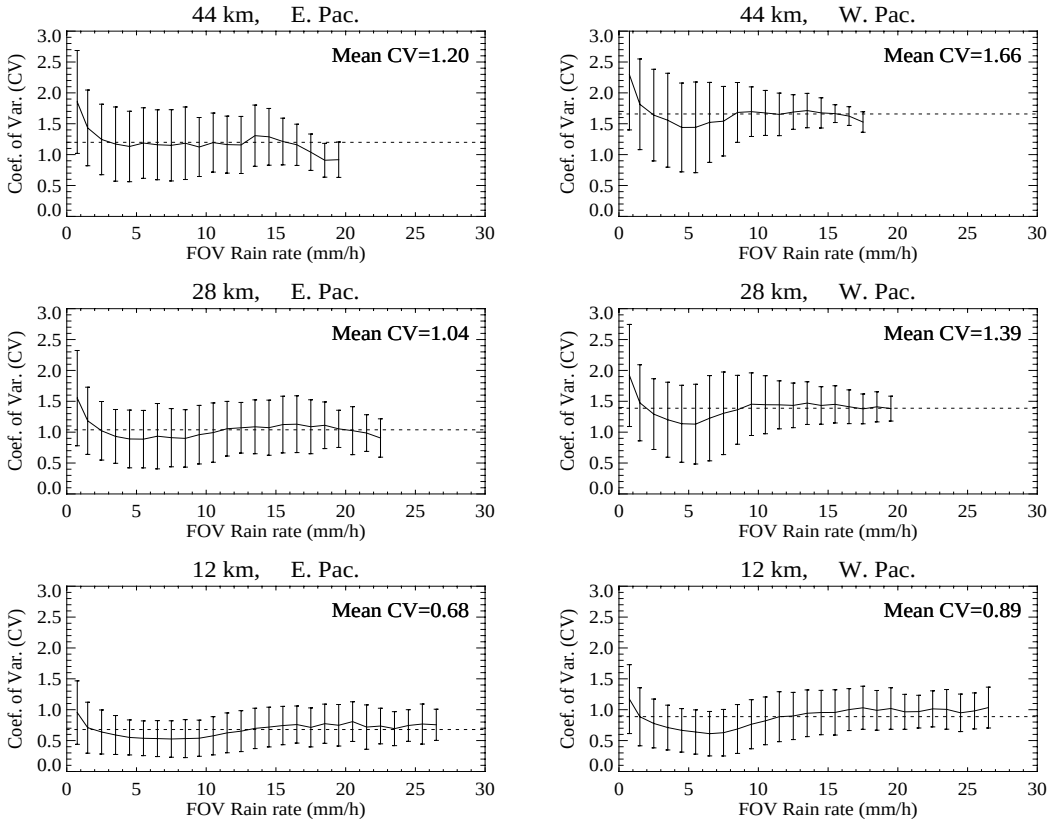

Figure 1: Variation of the coefficient of variation (CV) as a function of the FOV-averaged rain rate for the East and West Pacific. Each dotted line indicates the overall average of CV throughout the entire rain intensities.

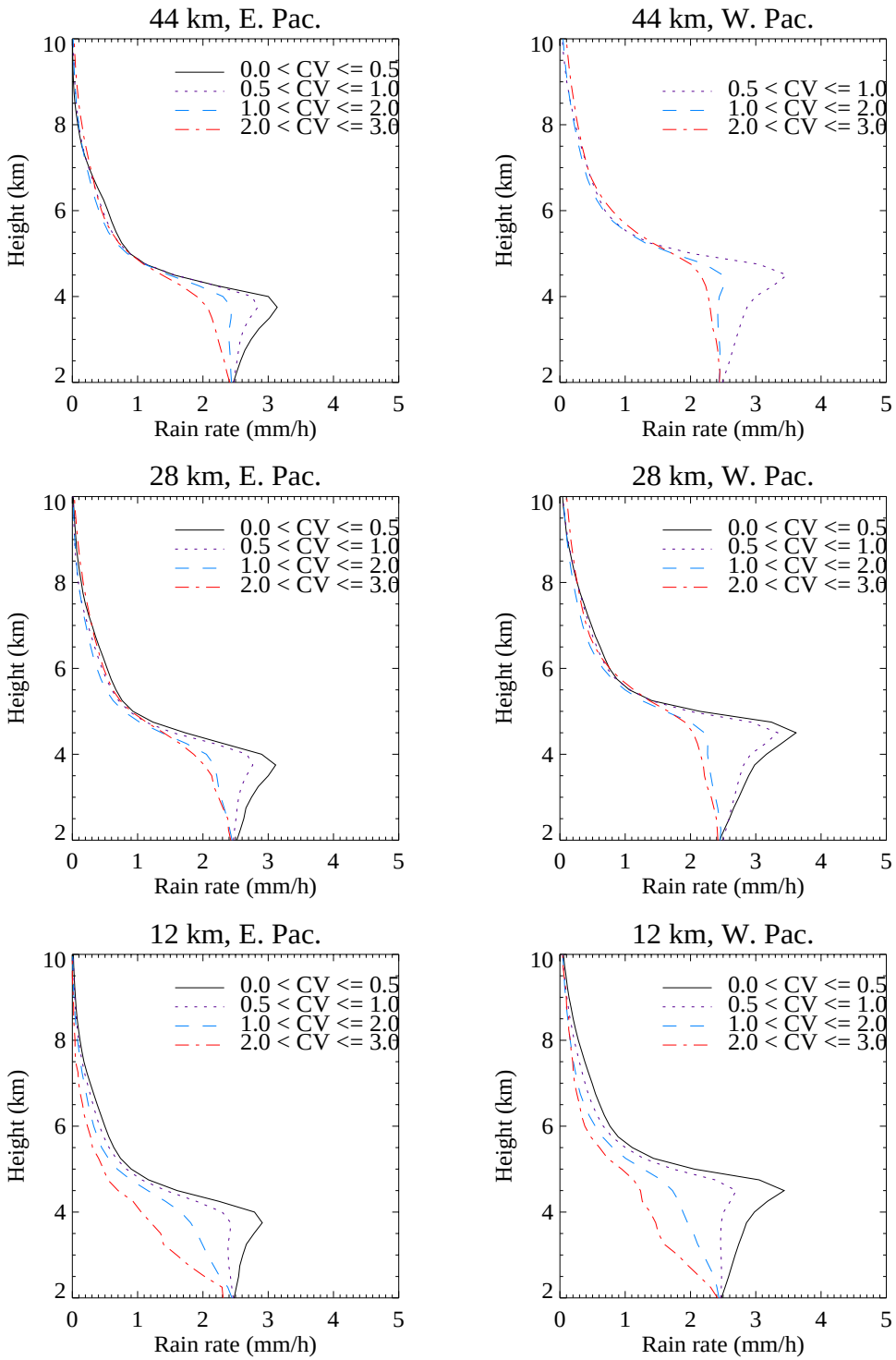

Figure 2: Vertical rainfall structures for different CVs with the same surface rain rate of 2.5 mm/h.

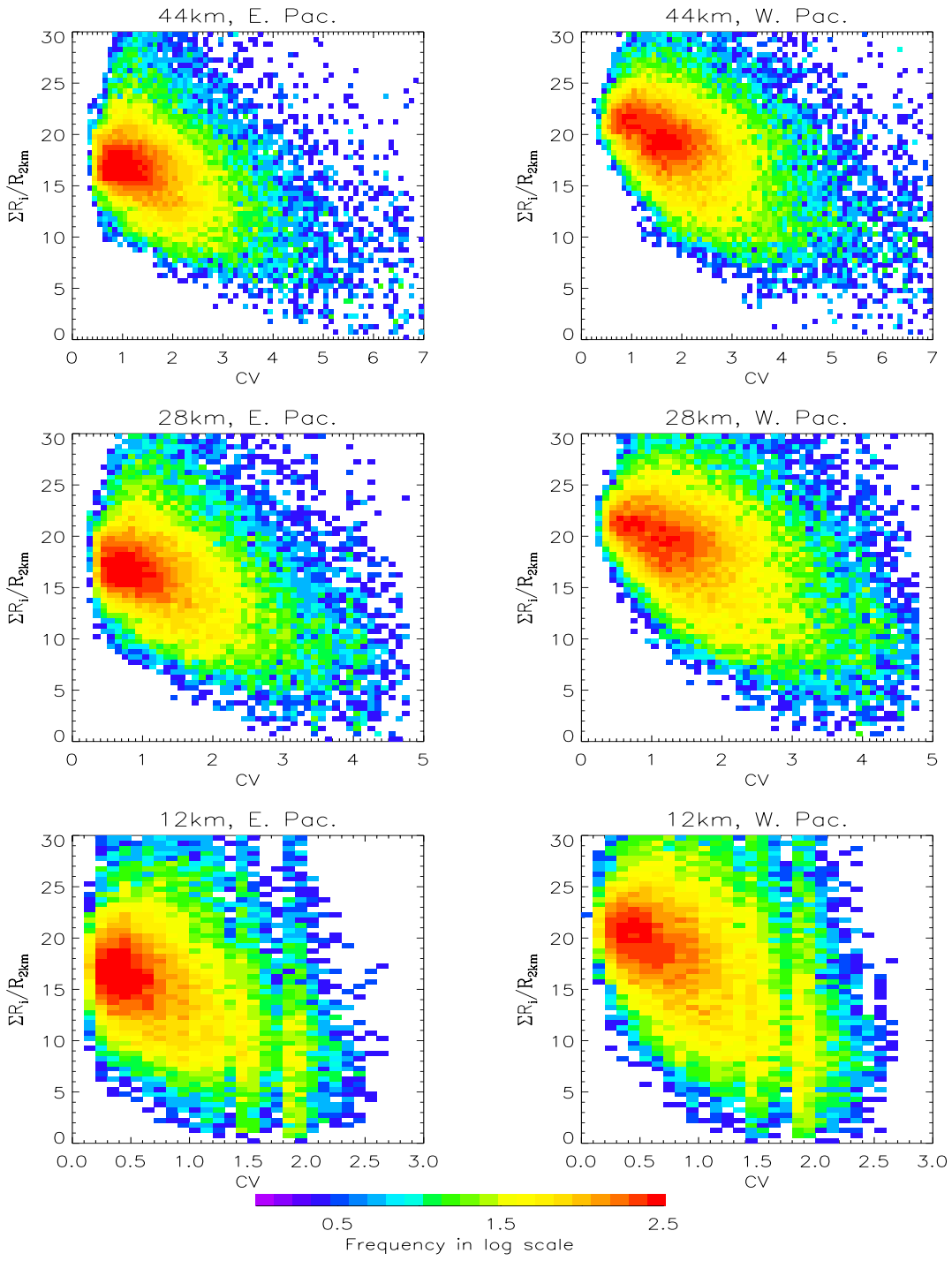

Figure 3: Two-dimensional histogram of CV and the ratio of total columnar rain rate (ΣR_i) to 2 km rain rate (R_{2km}).

4. RADIOMETRIC RESPONSES TO RAINFALL INHOMOGENEITY

Figures 4 and 5 show the observed relation between Tb and rain rate relations at the 4 different frequencies (horizontal polarization) as a function of the inhomogeneity factor for the East and West Pacific, respectively. The panels show the Tb-R relation for CVs ranges of 0-3. The Tb-R curve with the lowest CV (0-1) shows the highest retrieved rain rate on the Tb-R curve, i.e. lowest biases. The beam-filling biases increase with increasing CV. The differences between the curves are significant with increasing rain intensity at the frequencies where the effect of emission is dominant (10 and 19 GHz). The spatial inhomogeneity of rainfall also affects greatly the Tb-R relations at 37 GHz until the saturation reaches. The spatial resolution at 85 GHz approximately corresponds to the PR resolution so that the CV cannot be calculated. The dotted lines in these figures show the mean Tb-R curves. If we compare the mean Tb-R curves between the East and West Pacific, it can be seen that the mean curves for the East Pacific show a lower CV than those occurred in the West Pacific, due to the less inhomogeneous characteristics of rainfall over the East Pacific. As CV is correlated with the vertical structures, the differences of the Tb-R relations result from the coupling of the spatial inhomogeneity and correlated vertical structures of rainfall.

Figure 6 compares the mean Tb-R curves for the East and West Pacific. The upper/lower dotted lines show the +/- 1 standard deviation for the same rain rate category. From the emission channels (10 and 19 GHz) the difference of the relationship between the two regions is prominent with increasing rain intensity (above 6-7 mm/h). Here one may note that the rain-layer thickness is a major discriminator below about 4 ~ 5 mm/h, but uncertainty from inhomogeneous rainfall seems to have greater contribution to the difference above these rain rates. The West Pacific is characterized by higher freezing level than that of the East Pacific. This indicates that the West Pacific shows warmer Tbs with the same rain intensity than the East Pacific and it appears to be applicable to rain rates from 0 to about 4 ~ 5 mm/h. However as rain intensity increases, the larger inhomogeneity factor for the West Pacific compared to that of the East Pacific turns out to produce more nonlinearity in the relationship. It suggests that rainfall estimation based on emission property can have serious biases (consistent underestimates) over the regions with the considerable rain inhomogeneity in the FOV if it is not appropriately accounted for (Wilheit 1986).

The relationships at 37 GHz for the East and West Pacific show rapidly saturation and the difference between the two curves is clearly noticeable. At the scattering dominant frequency (85 GHz), where the rain inhomogeneity is not significant due to the high-spatial resolution, the Tb-R relation seems to be independent of the regions. The uncertainties are quite large, however. The similarity of the East and West Pacific Tb-R curve suggests only a weak link between frozen hydrometeors and liquid contents near the surface at the scattering frequencies.

5. DISCUSSIONS

In this study, we examine the response of the radiometric response of microwave sensor to the horizontal and vertical rain structures. Our objective is to provide further insight for error studies of passive microwave rainfall retrievals. Using the TRMM observations, we demonstrated that the uncertainty due to rainfall inhomogeneity is significant enough to weaken the relation between microwave brightness temperature and the vertically integrated liquid water content in clouds. It is also demonstrated that the horizontal inhomogeneity is typically correlated to the vertical structure. The combined effect contributes to increasing the uncertainty in the retrievals. These results are consistent with the approximate formula proposed by Chiu et al. (1990). The relatively stability of the CV over large rain rate regimes suggest that the beam-filling correction may be improved if information of the vertical structure (or rain type) are available.

Regional differences in the radiometric response are found between two climate regimes, the East and West Pacific. As rain rates and their spatial variability increases, as observed in the West Pacific, the unique radiometric signature seemed to be degraded significantly at the low frequencies where the effect of emission dominates, enhancing the nonlinearity in the physical connection. Thus, it is suggested that retrieval biases are dependent on climate regimes and rain type, where different horizontal and vertical precipitation structures exist.

Finally, it must be pointed out that in the Bayesian paradigm in which some rain algorithms, such as that adopted by the TRMM operational algorithm (2A12), the desired inference depends heavily on the prior knowledge of the radiometric response. For this reason, when cloud model simulations are used to establish *a priori* information, it is important to have the prior information as close to nature as possible. However, any perfect *a priori* information should first account for the errors due to the uncertainties inherent in both of the prior information and the retrieved rain field.

REFERENCES:

Chiu, L. S., G. R. North, D. A. Short, and A. McConnell, 1990: Rain estimation from satellites: Effect of finite field of view. *J. Geophy.Res.*, **28**, 2177-2185.

Kummerow, C., W. S. Olson, and L. Giglio, 1996: A simplified scheme for obtaining precipitation and vertical hydrometer profiles from passive microwave sensors. *IEEE Trans. Geosci. Remote Sens.*, **34**, 1213-1232.

_____, W. Barnes, T. Kozu, J. Shiue, and J. Simpson, 1998: The Tropical Rainfall Measuring Mission (TRMM) sensor package. *J. Atmos. and Ocean Technol.*, **15**, 808-816.

Petty, G., W., 1994: Physical retrievals of voer-ocean rain rate from multichannel microwaver imagery. Part I: Theoretical characteristics of normalized polarization and scattering indices. *Meteor. Atmos. Phys.*, **54**, 79-99.

Shin, D.- B., and C. Kummerow, 2002: Parametric rainfall retrieval algorithms for passive microwave radiometers. Submitted to *J. Atmos. and Ocean Technol.*

Smith, E. A., and A. Mugnai, 1988: Radiative transfer to space through a precipitating cloud at multiple microwave frequencies. Part II: Results and analysis. *J. Appl. Meteor.*, **27**, 1074-1091.

Spencer R., H. M. Goodman, and R. E. Hood, 1989: Precipitation retrieval over land and ocean with the SSM/I: Identification and characteristics of the scattering signal. *J. Atmos. and Ocean Technol.*, **6**, 254-273.

Wilheit, T. T., A. T. C. Chang, M. S. V. Rao, E. B. Rodgers, and J. S. Theon, 1977: A satellite technique for quantitatively mapping rainfall rates over the oceans. *J. Appl. Meteor.*, **16**, 551-560.

_____, 1986: Some comments on passive microwave measurement of rain. *Bull. Bull. Amer. Meteor. Soc.,* **67**, 1226-1232.

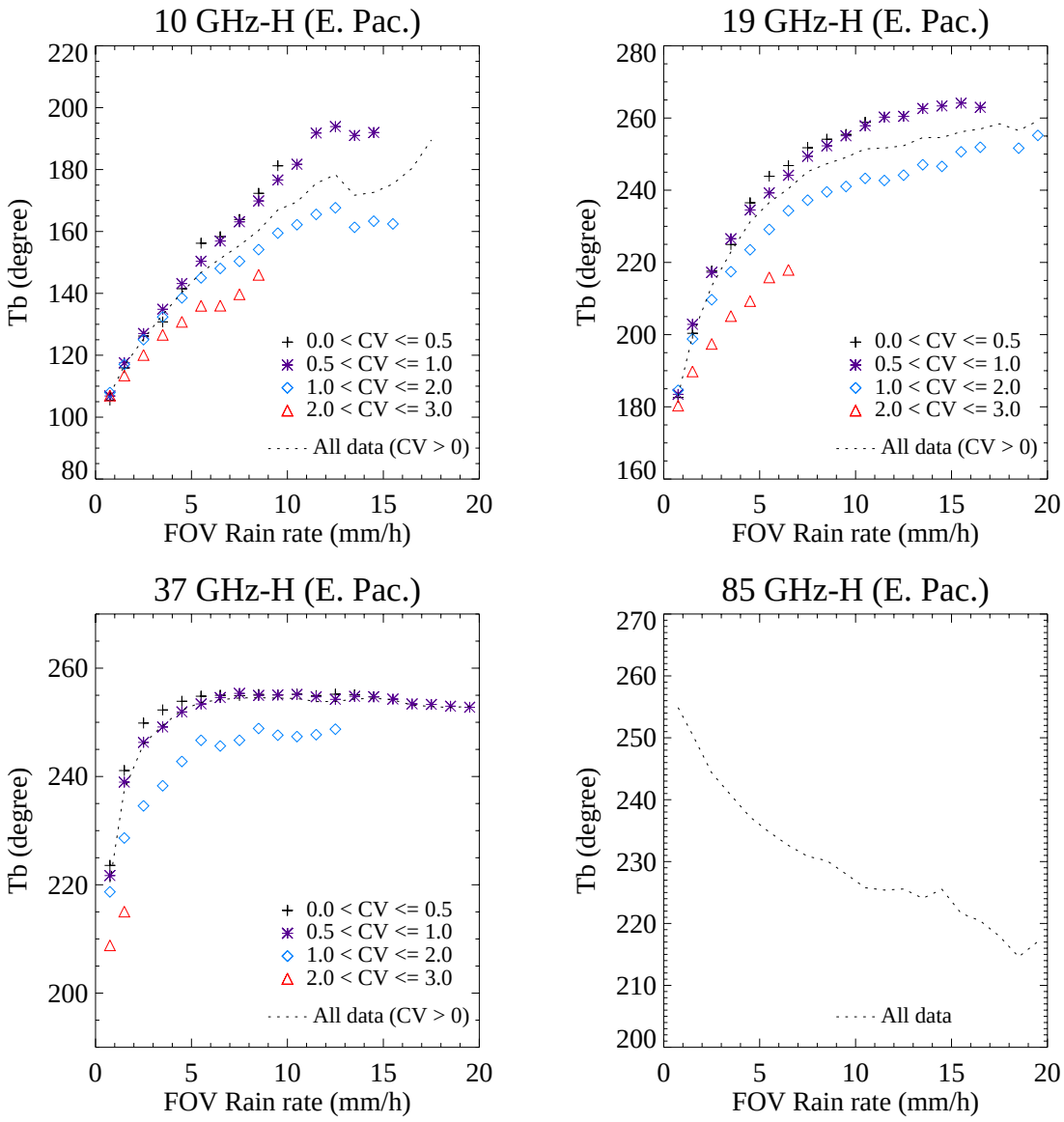

Figure 4: Relationship between brightness temperature (Tb) and rain rate as a function of FOV-averaged CV at four different horizontally polarized channels of TMI over the East Pacific.

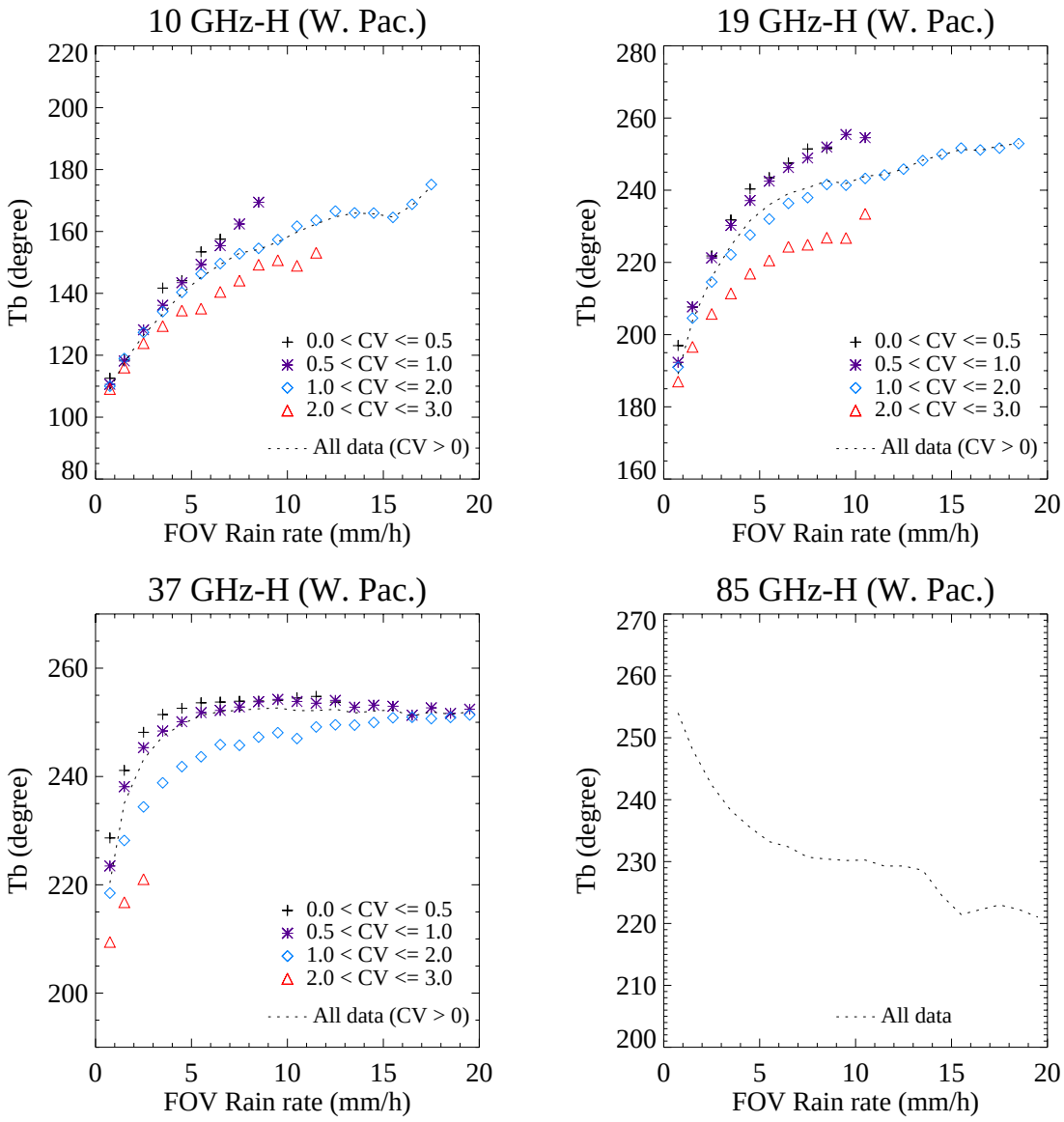

Figure 5: Same as Fig. 4 but for the West Pacific.

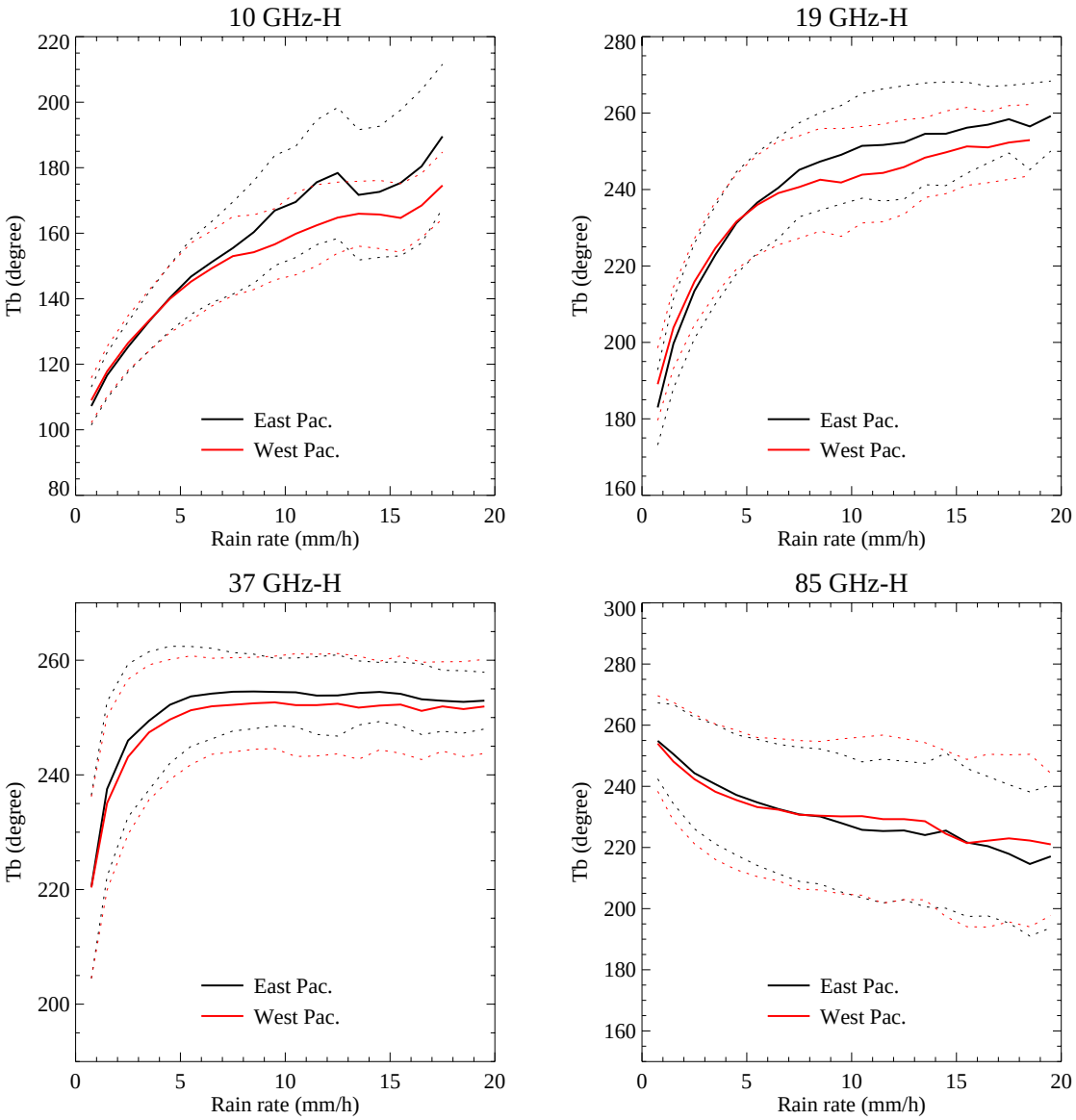

Figure 6: Relationship between brightness temperature (Tb) and rain rate at the horizontally polarized 10, 19, 37 and 85 GHz channels of TMI for the East and West Pacific. The upper and lower dotted curves show the +/-1 standard deviation of Tb (dotted line) at the various rain intensities.